Time Resolved Ultraviolet Spectroscopy of DQ Herculis: Eclipses and Pulsations[1]

Andrew D. Silber, Scott F. Anderson, Bruce Margon
Astronomy Dept., University of Washington, Box 351580, Seattle, WA 98195-1580, USA;
silber@astro.washington.edu,margon@astro.washington.edu, anderson@astro.washington.edu

and

Ronald A. Downes
Space Telescope Science Institute, 3700 San Martin Drive, Baltimore, MD 21218, USA;
downes@stsci.edu

ABSTRACT

The magnetic cataclysmic variable DQ Herculis was observed with the Faint Object Spectrograph onboard the Hubble Space Telescope (HST) over four consecutive satellite orbits, including the first observation in the UV of DQ Her through eclipse minimum. Strong emission in N V, C IV, Si IV, and He II and weak emission in O I, S III, Ni II, N IV, Si III, and C III was seen.

Time resolved spectroscopy was obtained over 3 orbits with the G160L grating. At the eclipse minimum, the UV continuum was completely eclipsed for $< 5\%$ of the orbital period. This implies that the UV continuum emission region is very compact. By contrast, none of the emission lines were completely eclipsed, most notably C IV which dropped by only $\sim 75\%$.

DQ Her is known to have intermittent pulsations in the optical and UV at a period of 71 s, due to the rotation of the accreting white dwarf. As in our previous observations, the UV continuum and the C IV emission show sporadic 71 s pulsations. The mechanism(s) which determine the pulsation amplitudes are clearly complex.

The strong emission lines and continuum were auto-correlated during the first and third HST orbits and all show a variability timescale of ~ 160 s. The intensities of these lines were also cross-correlated with the continuum and show a strong correlation with the continuum with a timelag of ≤ 4 s.

The data during the fourth HST orbit were collected with the G190H grating ($\lambda\lambda$ 1600-2350 with 1.5 Å spectral resolution) in standard spectroscopy mode (240 s time resolution). These observations resolve He II λ 1640 into a broad (1,400 km s^{-1}), asymmetric line.

Subject headings: Ultraviolet:Stars - Stars:Cataclysmic Variables - Stars:Individual:(DQ Herculis)

---

[1] Based on observations with the NASA/ESA Hubble Space Telescope obtained at the Space Telescope Science Institute, which is operated by the Association of Universities for Research in Astronomy, Inc., under NASA contract NAS5-26555.

1. Introduction & Observations

Cataclysmic variables (CVs) are semi-detached binary systems consisting of a red dwarf (the secondary star) that fills its Roche-lobe and a white dwarf (the primary) that accretes matter from the secondary star. DQ Herculis is the prototype of those stars in which the magnetic field of the white dwarf plays a significant, but not overwhelming, role (Patterson 1994). The accreting material forms a disk around the white dwarf, but this disk is disrupted by the white-dwarf's magnetic field before reaching the surface. In some DQ Her systems the magnetic field may even disrupt the entire accretion disk (e.g. Hellier 1991). Unlike the highly magnetic AM Her type CVs in which the white dwarf rotates in (or nearly in) synchrony with the orbital period, the white dwarf in DQ Her stars is spinning more quickly than the orbit, due to accretion torques.

Stable pulsations at a period distinct from the orbital period are the defining observational property of DQ Her type CVs. These pulsations originate on the white dwarf at a bright spot where the magnetically funneled accreting material strikes the white-dwarf surface. The high temperature and density of the accreting material leads to a high efficiency of X-ray emission and the highest amplitude of the pulsations is often in the X-rays. Some of this emission may be reprocessed elsewhere in the system (e.g. the accretion disk or the secondary star) which can lead to pulsations in the optical at one or more of the beat periods between the orbit and spin periods (Warner 1986).

DQ Her itself shows pulsations in the optical broad band emission (e.g. Walker 1956), the HeII λ 4686 line (Chanan, Nelson, & Margon 1978; Martell et al. 1995), and the UV continuum and several UV emission lines (Silber et al. 1996; hereafter Paper I). All of the optical pulsation amplitudes vary with time in a complicated manner. In this paper we will show that this is also true of the UV pulsations.

DQ Her itself is only very weakly detected in soft X-rays (Paper I), and there is no evidence of pulsations in the X-rays. Most likely this is due to the accretion disk blocking a direct view of the white dwarf, as would be expected in a system with an inclination this high ($i = 86.5°$; Horne, Welsh, & Wade 1993).

DQ Her was observed with the Faint Object Spectrograph (FOS) on the Hubble Space Telescope over 3 consecutive orbits on 27 April 1995 (post-refurbishment) from 17:09 to 20:52 UT (Table 1). These data were collected with the $0.9''$ aperture and the G160L grating in the "rapid" mode, with 3.9 s integrations and with spectral resolution of about 7 Å. The total integration time was 5,770 s. We also observed DQ Her for one HST orbit with the G190H grating (from 22:02:02 to 22:42:02) in the standard spectroscopy mode, just after the G160L data were collected. These data have a spectral resolution of about 1.5 Å and time resolution of 245 s and were also collected through the $0.9''$ aperture.

Times in this paper are Heliocentric Julian Date minus 2449800. The orbital phase is given using the linear ephemeris of Zhang et al. (1995). The spin ephemeris used is a linear ephemeris derived from Zhang et al.'s (1995) cubic ephemeris brought to the epoch of our observations:

$$T_{max} = 35.3255 + 0.000822(E). \quad (1)$$

2. Spectrum

The average spectrum of data collected with the G160L grating (Fig. 1 and Table 2) shows strong emission of N V, C IV, Si IV/OIV], and He II. Higher-resolution UV spectra taken with the FOS suggest that the Si IV emission dominates the Si IV/O IV] complex (Eracleous, private communication). The emission from Lyα is greatly reduced compared to the previous observation (Paper I) where it was concluded that there was significant contamination from geocoronal emission.

Weak lines of O I (1304 Å) or S III] (1298 Å), Ni II (1346), Ni II (1460 Å), N IV (1722 Å), Si III (1892 Å), and C III (2297 Å) are also seen. There are many even weaker features, especially from 1800 to 2000 Å. Except for the drop in Lyα emission (which is probably explained by changes in the geocoronal contamination), the spectrum is quite similar to that seen in Paper I, though the strong emission lines are more intense in these more recent observations. This brightening cannot be explained by different orbital sampling because these data do not include the phase when the hotspot is visible (and the spectrum is brightest) and do include the eclipse minimum (when the spectrum is faintest).

The lower spectrum of Fig. 1 shows the spectrum during the eclipse. From this it is clear that the UV continuum is completely eclipsed while the lines are affected to differing degrees. We will discuss this further in §3.

In Paper I we were unable to create a spectrum of reasonable match to the observations of strong Lyα, N V, Si IV (or OIV]), C IV, and He II, emission using the photoionzation code *xstar* (Kallman & McCray 1982; Krolik & Kallman 1984; Kallman & Krolik 1986). We have reconsidered this issue, removing the requirement for strong Lyα. In none of the models are the combination of N V, Si IV (or O IV]), C IV, and He II among the 6 strongest lines. Again the most serious problem is the inability of the models to predict a strong Si IV line. In Paper I one possible explanation given was that new calculations of the charge transfer process might increase the production of Si IV. Preliminary explorations of this suggest that the latter process does not significantly increase the production of Si IV 1400 Å (Kallman, pvt. comn).

In the G190H spectrum (Fig. 2) we see that the weak lines N IV 1722 Å, Si III 1892 Å, and C III 2297 Å are even more apparent than they were in the low resolution data. Additionally there are many weak features in the G190H data that we are unable to unambiguously identify. These lines are not due to flat-field features in the detector because they are also visible in the G160L data (including the rich complex of features from 1800 to 2000 Å). One possible source of some of the weak features is Fe III in emission, but a number of the expected lines are seen in absorption or not at all.

The only strong line included in the G190H data is He II 1640 λ (Fig. 3). This line is clearly resolved with a FWHM of 7.7 Å (1,400 km s^{-1}), and an asymmetric profile with a steeper rise on the blue side. This is similar to the profile of He II λ 4686 (Martell et al. 1995). There is no clear variability in the centroid wavelength or line width of He II over the one HST orbit, but the integrations are too long to show the short timescale variability seen in the "rapid" mode data and the coverage is to short to show orbital variations.

3. Time Variability

In Figure 4 we show the flux of the 5 strongest UV lines and the continuum from the "rapid mode" data. The most striking feature is the eclipse in the center of the second HST orbit. The UV eclipse time is consistent with the expected time of the optical eclipse. Two issues complicate a detailed analysis of the eclipse profile (e.g. eclipse mapping; Horne 1985): the lack of complete phase coverage; and the uncertain, but significant, self-occultation by the convex accretion disk. Nonetheless, we can draw some conclusions from the eclipse profile. The symmetry between the ingress and egress argues that the emission region has a line of symmetry along the line connecting the two stars. The sloping ingress and egress require that the emission regions are extended: the continuum egress lasts > 4 % of the orbit, which implies a size of $> 1.4 \times 10^{10}$ cm assuming the orbital parameters of Horne et al. (1993) and that the emission is centered on the white dwarf. The bulk of the continuum emission region is eclipsed from 35.286 to 35.295 (about 5% of the orbital period). If we ignore the blockage of the white dwarf by the disk, the predicted duration of the white dwarf eclipse is slightly longer than the observed UV continuum eclipse, hence the UV continuum eclipse duration is short, and the size is small.

While the UV continuum is completely eclipsed, the same cannot be said for the emission lines. The eclipse for He II is nearly complete, while the eclipse for N V and Si IV are deep, but not complete. Lyα also is partially eclipsed, but due to the low signal-to-noise and uncertain geocoronal contamination it is unclear what fraction of the emission from DQ Her is eclipsed. The most interesting case is C IV, which only drops by about 75%, showing significant emission even at the minimum. Clearly the line emission regions are larger than the secondary. If we treat the emission region as a uniform sphere (reasonable for setting lower limits) and adopt the secondary size given in Horne et al. (1993), the C IV comes from a region with a radius of $> 4 \times 10^{10}$ cm. Evidence that C IV comes from an extended region has been seen in other systems (e.g. OY Car; Horne et al. 1994) as well.

4. Auto- and Cross-Correlations

We performed auto-correlations of the line and continuum emission during the first and third (non-eclipse) HST orbits separately (Table 3 and Figure 5). These correlations were normalized such that the value is unity at zero time lag. The results from the two HST orbits are similar. The auto-correlation of the continuum slopes from a maximum at zero time lag to a plateau at a lag time of 160 s. This is similar to what is seen in the optical by Schoembs & Rebhan (1989). The shape of the auto-correlation for the strong emission lines is similar to that of the continuum, except that each of the lines has a peak at zero timelag caused by counting noise which is only correlated at zero timelag. This effect is not important for the continuum because of the much higher signal-to-noise ratio. The auto correlation of Lyα is flat, with a spike at zero timelag. This suggests that the variability of Lyα is dominated by noise, which would not be correlated at non-zero timelags, rather than a physical process (e.g. flickering), which is correlated at small timelags for the other lines. In Table 3 we list the timescale at which the auto-correlations flatten.

We cross-correlated the emission from the lines with the continuum (Figure 5). The Lyα

emission shows no correlation with the continuum. All of the other lines are correlated with the continuum at a high level with a time delay of ≤ 4 s. This difference further suggests that the variability in Lyα is dominated by noise.

5. The Spin Period

In Paper I, intermittent pulsations at the white-dwarf spin period (or half the spin period; Zhang et al. 1995) were detected in the UV continuum, C IV, and Lyα emission. We performed a search for pulsations and upper limits (Table 4) at the 71-s period on these newer data as described in Paper I. Amplitude and period errors are estimated via a Monte Carlo simulation as discussed in Silber et al. 1992. The second HST orbit was split into 3 sections: eclipse ingress (T <35.285); eclipse ($35.285 < T < 35.297$); and eclipse egress ($T > 35.297$). No pulsation upper limits are given during HST orbit 2 because of the short duration of the segments and the lower signal-to-noise.

During the first HST orbit the only pulsation detected at the 71-s period was in the continuum (Fig. 6). This pulsation with an half amplitude of 1.6 ± 0.6 % was at 71.3 ± 0.8 s, consistent with the expected period of 71.0 s. During the third orbit, C IV was seen to vary at 71.1 ± 0.5 s with an half amplitude of 4.7 ± 1.1 %. C IV is also seen to pulse (after removing a linear trend) during the eclipse ingress at a period of 68.7 ± 1.3 s and at an half amplitude of $(1.0 \pm 0.3) \times 10^{-13}$ ergs s^{-1} cm^{-2}. It is unclear whether this pulsation is just due to noise in a short data set or the rotation of the white dwarf. In Fig. 7 we see each of these datasets folded with the ephemeris in Eq. 1. (1995). We see that the maximum flux from the UV continuum during the first and the C IV line during third HST orbit are maximum at the same phase as the predicted phase of the optical data. This is contrary to what was seen in Paper I for C IV. As we have no reason to favor one data set over the other, we infer that the phase of maximum UV flux is yet another parameter which varies in a complex fashion.

6. Summary & Discussion

DQ Herculis was observed with the HST FOS for three satellite orbits in April 1995. The spectra were obtained in the "rapid" mode with 3.9 s time resolution. The mean spectrum shows strong emission from N V, Si IV, C IV, and He II. These lines are brighter ($\sim 50\%$) than in our October 1993 observations (Paper I). Unlike our 1993 observations the Lyα emission is weak, suggesting that a major source of Lyα in the earlier observation was geocoronal, as we previously inferred. Photoionzation models have difficulty producing the observed Si IV emission.

These data include the first observation in the UV through eclipse minimum. During the eclipse of the accretion disk, the UV continuum emission drops to zero; this emitting region must be quite compact. While the continuum is disappearing, C IV, the strongest line, and N V drop by $\sim 75\%$. He II and Si IV are more strongly eclipsed, but even these lines are still seen at the center of the eclipse. Clearly the emission lines come from a region significantly more extended than the continuum. Whatever produces these lines must be larger than the secondary.

From optical studies (e.g. Chanan et al. 1978; Young & Schneider 1980) we know that the Balmer lines and He II λ 4686 are dominated by disk emission. The optical continuum is completely eclipsed, while Hβ is eclipsed by about 75% (Martell et al. 1995). Hγ and He II λ 4686 are also deeply, though not completely, eclipsed. Hence the behavior in the UV is similar to that seen in the optical.

The high level of the cross-correlation between the UV continuum and the lines argues that the emission between the two is tightly coupled, even though the eclipse requires that the emission regions are physically distinct (though possibly overlapping). The similar timescale of the auto-correlation also argues for a relation between the variability of the UV lines and continuum. What is unclear is cause and effect: are the lines brightened by reprocessed UV continuum emission; are both caused by inhomogeneities in the accretion; or are both reprocessed X-ray emission? The larger size of the line emission region suggest that reprocessing is part of the answer. As the light travel time across the white-dwarf Roche lobe is about 3 s, higher time resolution is needed to answer this question.

Coherent pulsations at the 71 s spin period are seen in the UV continuum, but only during the first HST orbit. C IV is seen to pulse during the third HST orbit. The phasing of both of these pulsations is consistent with that of the optical pulsations. There is also a possible detection of pulsations in C IV during the eclipse ingress. Our previous observations of DQ Her also showed intermittent pulsations of the UV continuum and emission lines. These observations raise the question of what factor(s) control the complex behavior of the pulsation amplitudes. Even after four decades of observations in the optical, the mechanism that controls the amplitude of these pulsations is unknown. What is clear from our data is that the UV behavior is at least equally complex.

This work was supported by NASA Grant NAG5-1630.

Table 1. Observation Summary

HST Orbit	Start [JD-2449800]	Duration [s]	Time Resolution[s]	Grating	ϕ_{orbit}
1	35.22	1923	3.9	G160L[a]	0.67
2	35.28	1923	3.9	G160L[a]	0.01
3	35.35	1923	3.9	G160L[a]	0.33
4	35.42	2454	245	G190H[b]	0.72

[a] $\lambda\lambda 1150 - 2500$, $\lambda/\Delta\lambda = 260$

[b] $\lambda\lambda 1600 - 2350$, $\lambda/\Delta\lambda = 1300$

Table 2. DQ Her Ultraviolet Emission Lines in the Time-Averaged Spectrum

	Lyα	N V	Si IV	C IV	He II[a]
Flux[b]	2.4	4.2	5.7	16.4	3.0 (3.3)
EW[Å]	35	63	86	201	43 (36)
Wavelength[Å]	1218	1246	1402	1552	1643 (1641)
FWHM[Å]	20	12	19	14	11 (8)

[a] The values in parenthesis are from the fourth HST orbit (G190H data). All the other data is from the combined G160L spectrum.

[b] 10^{-13} ergs s^{-1} cm^{-2} Å^{-1}

Table 3. Auto-Correlations Timescale

Line	Orbit 1 [s]	Orbit 3 [s]
Continuum	160	160
N V	160	140
Si IV	160	200
C IV	150	180
He II	160	180

Table 4. Pulsation Upper Limits

Line	HST Orbit 1 [%]	HST Orbit 3[%]
Lyα	30	25
N V	6	10
Si IV]	8	10
C IV	4	N/A
HeII	6	9
Continuum	N/A	2

REFERENCES

Chanan G.A., Nelson J.E. & Margon B. 1978, ApJ, 226, 963

Hellier, C. 1991, MNRAS, 251, 693

Horne, K. 1985, MNRAS, 213, 129

Horne K., Marsh T.R., Cheng F.H., Hubeny I. & Lanz T. 1994, ApJ, 426, 294

Horne K., Welsh W.F. & Wade R.A. 1993, ApJ, 406, 229

Kallman, T. R. & Krolik, J. H. 1986, ApJ, 308, 805

Kallman, T. R. & McCray, R. 1982, ApJS, 50, 263

Krolik, J. H. & Kallman, T. R. 1984, ApJ, 286, 366

Martell P.J., Horne K., Price C.M. & Gomer R.H. 1995, ApJ, 448, 380

Patterson J. 1994, PASP, 106, 481

Schoembs R. & Rebhan H. 1989, A&A, 224, 42

Silber A., Bradt H.V., Ishida M., Ohashi T. & Remillard R.A. 1992, ApJ, 389, 704

Silber, A., Anderson, S. F., Margon, B., & Downes, R. 1996, ApJ, 462, 428 (Paper I)

Walker M.F. 1956, ApJ, 123, 68

Warner, B. 1986 MNRAS, 219, 347

Young P. & Schneider D.P. 1980, ApJ, 238, 955

Zhang, E., Robinson, E. L., Stiening, R. F., & Horne, K. 1995, ApJ, 454, 447

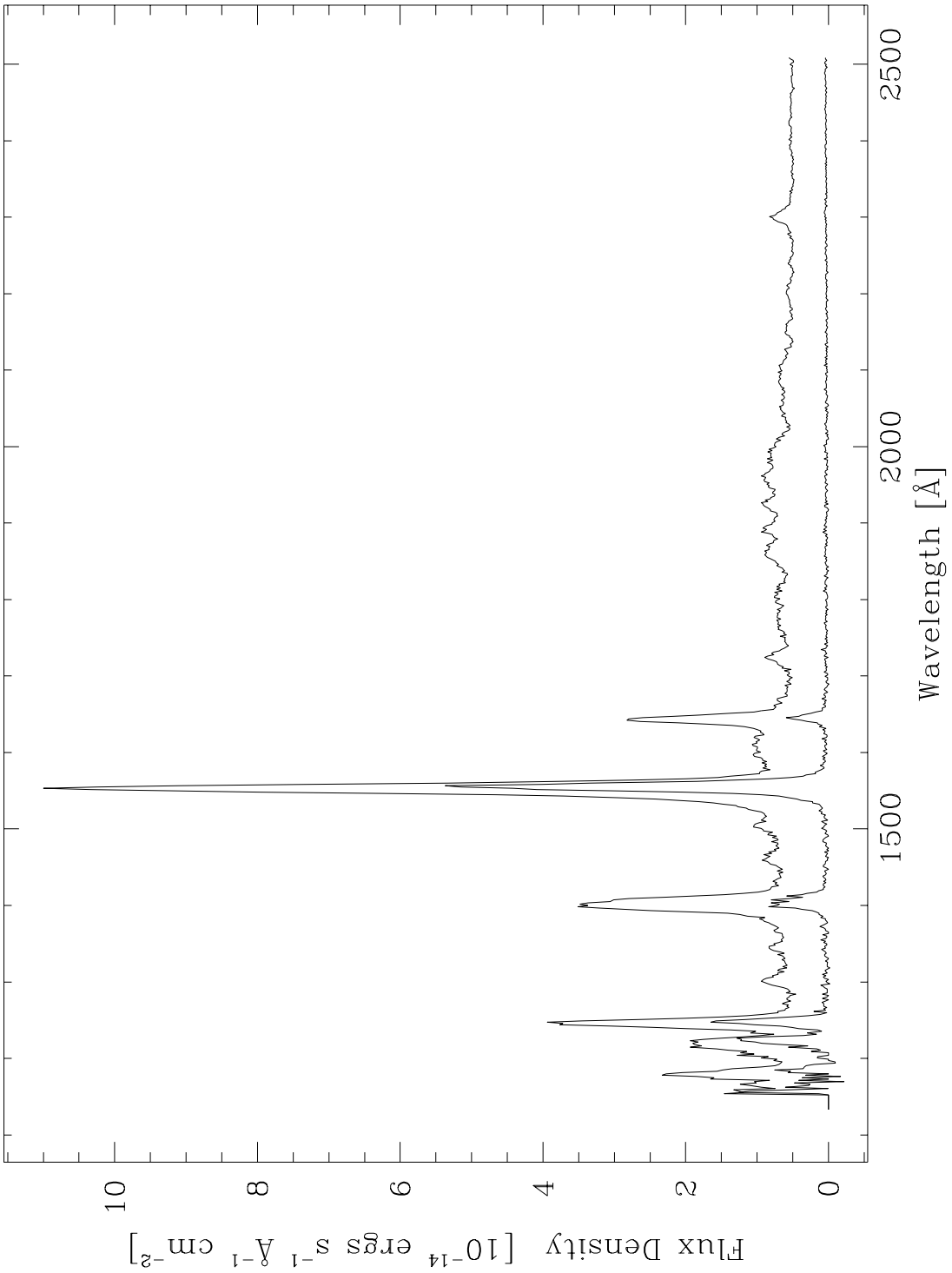

Fig. 1.— *Upper curve:* The total integrated spectrum of DQ Her with the G160L grating. Note the strong C IV, Si IV, N V, and He II emission. The strong Lyα emission seen during the previous visit to DQ Her (Paper I) is not seen, possibly due to long term variability in the emission from this line or, more likely, variation in the contamination by the geocoronal emission. *Lower curve:* The spectrum during the eclipse ($35.285 < T < 35.297$). During the eclipse the continuum emission region is completely blocked while some line emission is still visible, especially for C IV.

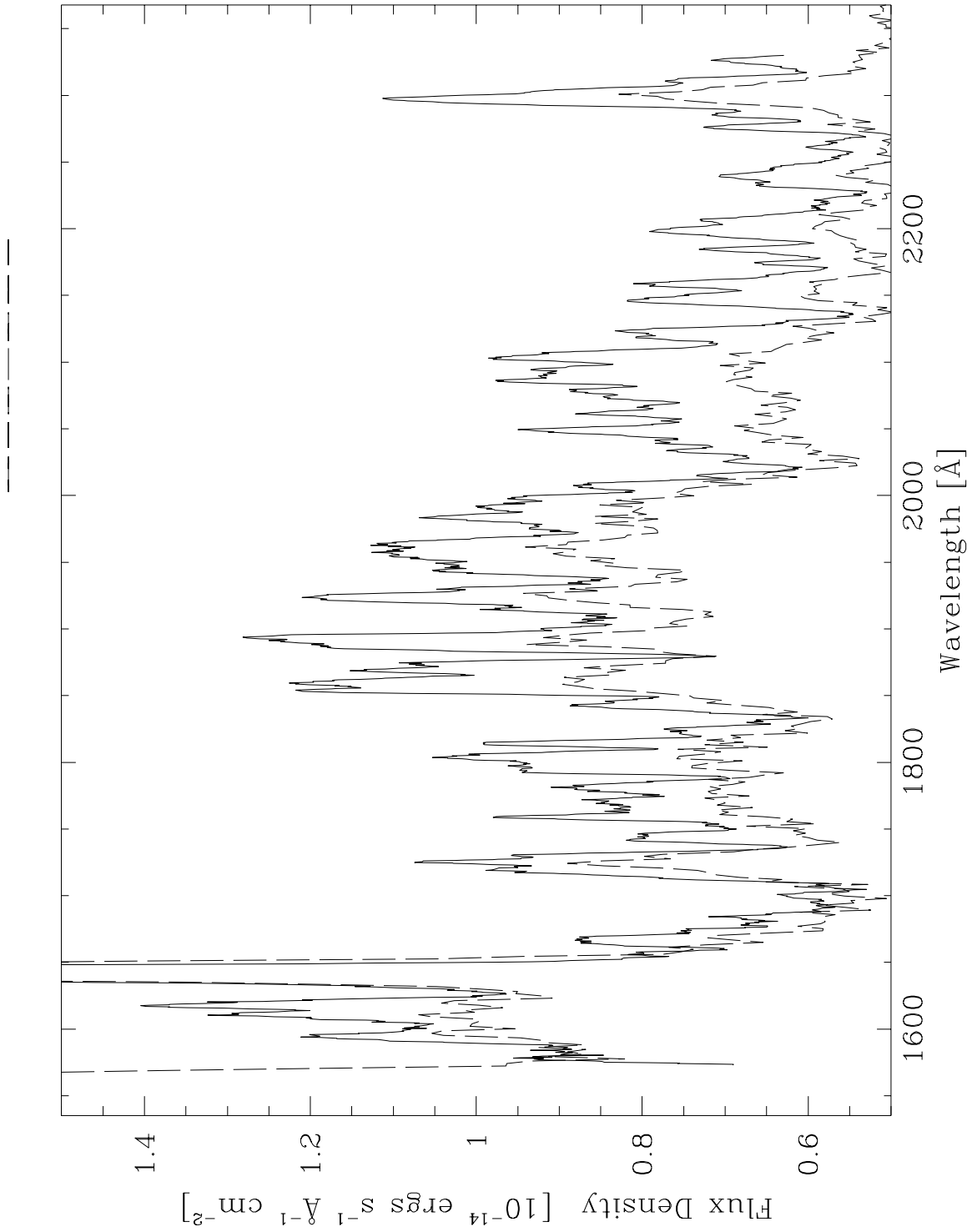

Fig. 2.— The spectrum from the G190H (solid) scaled to show the weak features including N IV (1722 Å), Si III (1892 Å), and C III (2297 Å). Numerous weaker features are also apparent and unidentified, especially in the 1800 to 2000 Å range. We also show the G160L data (dashed) which has a lower resolution, but shows the same features.

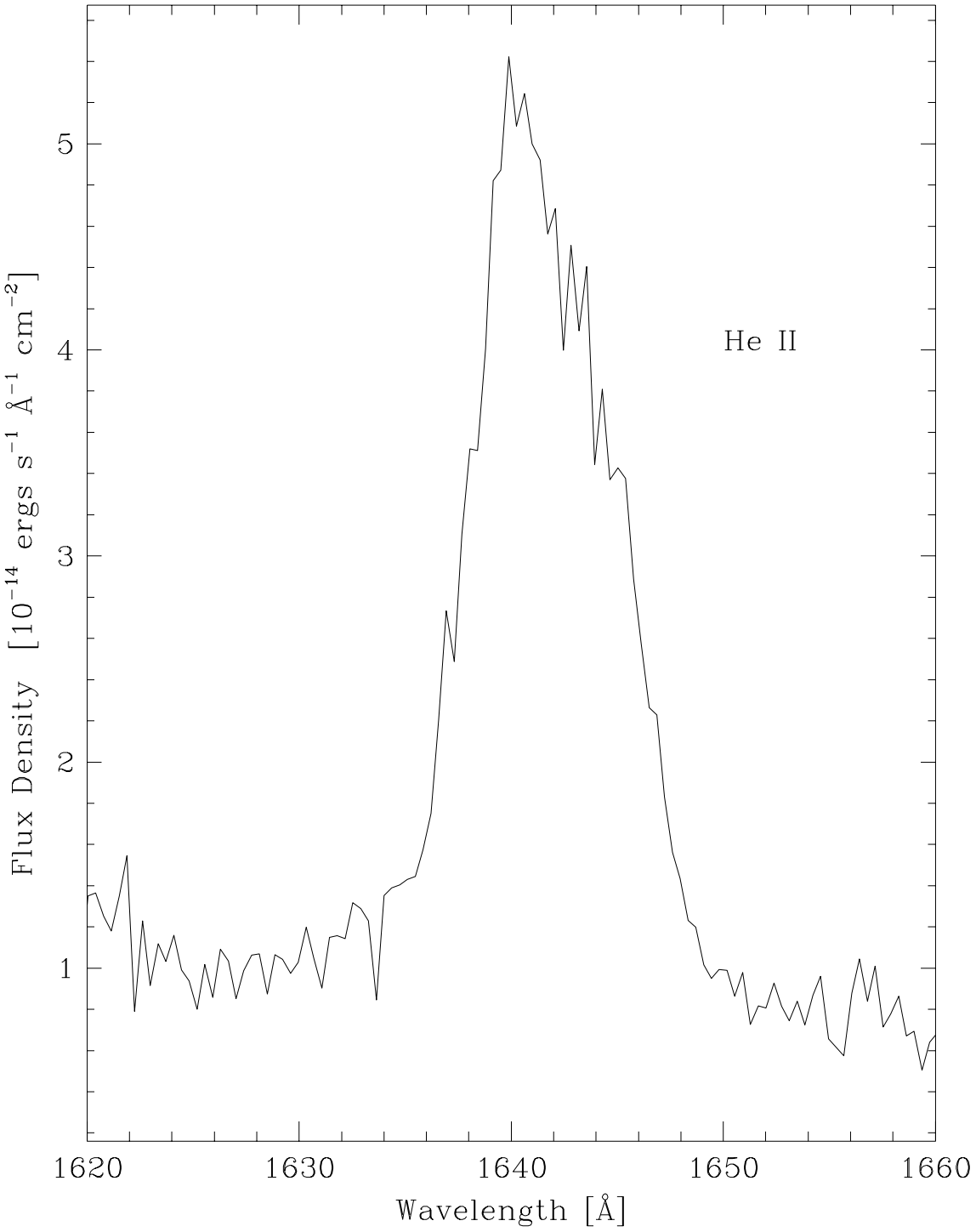

Fig. 3.— An expansion around He II of the G190H spectrum. The line is well resolved with a FWHM of 7.7 Å, compared to the instrumental resolution of 1.5 Å. The rise in the blue wing is much steeper than that in the red.

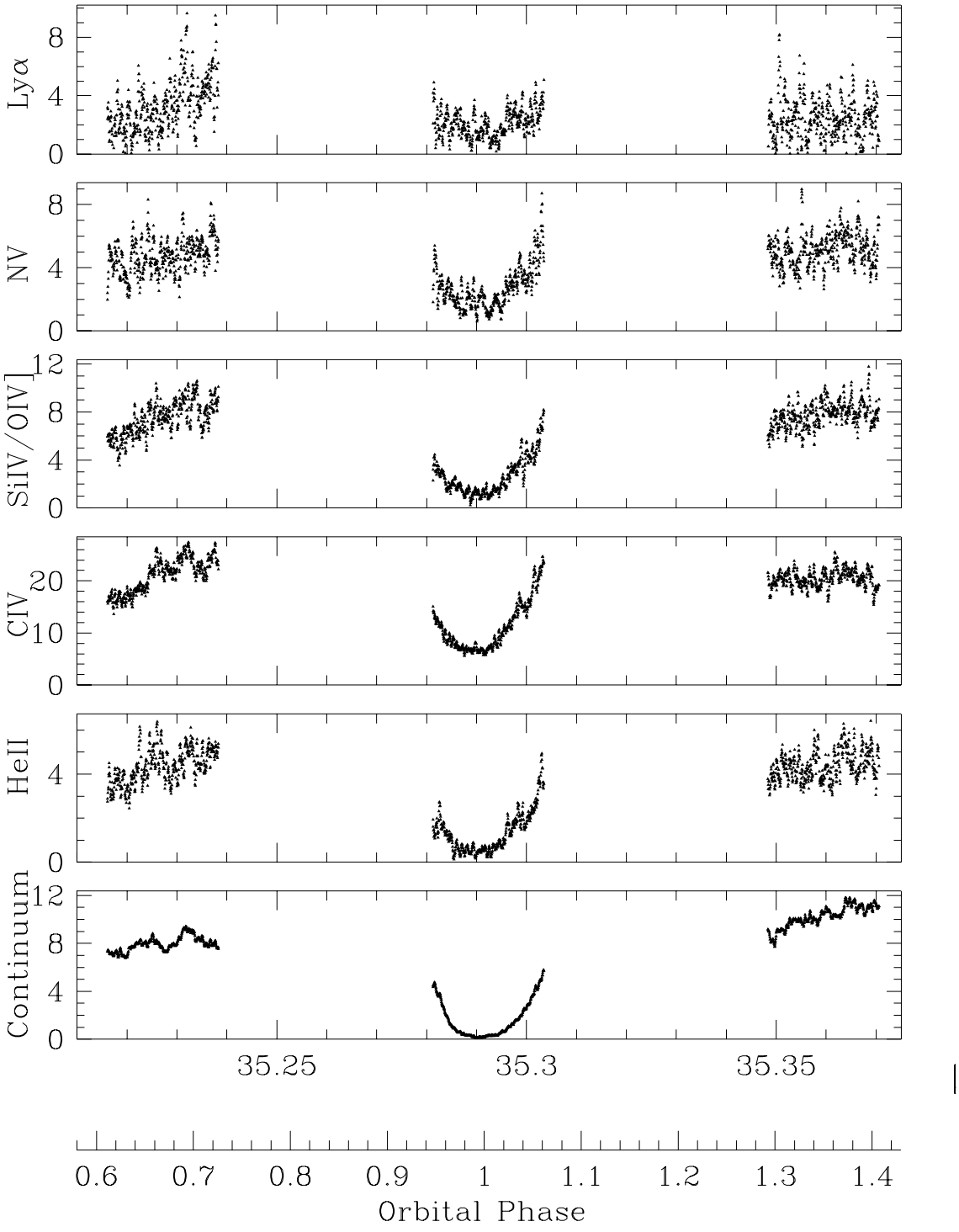

Fig. 4.— The flux in the 5 strongest lines and the continuum as a function of time. The continuum includes the flux from weak lines (e.g. O I, C III). The eclipse time in the UV continuum is consistent with the optical eclipse ephemeris. The line fluxes are significantly, but not completely, diminished during the eclipse. There is flickering in both the lines and continuum, which by inspection can be seen to be correlated, most clearly in the first HST orbit.

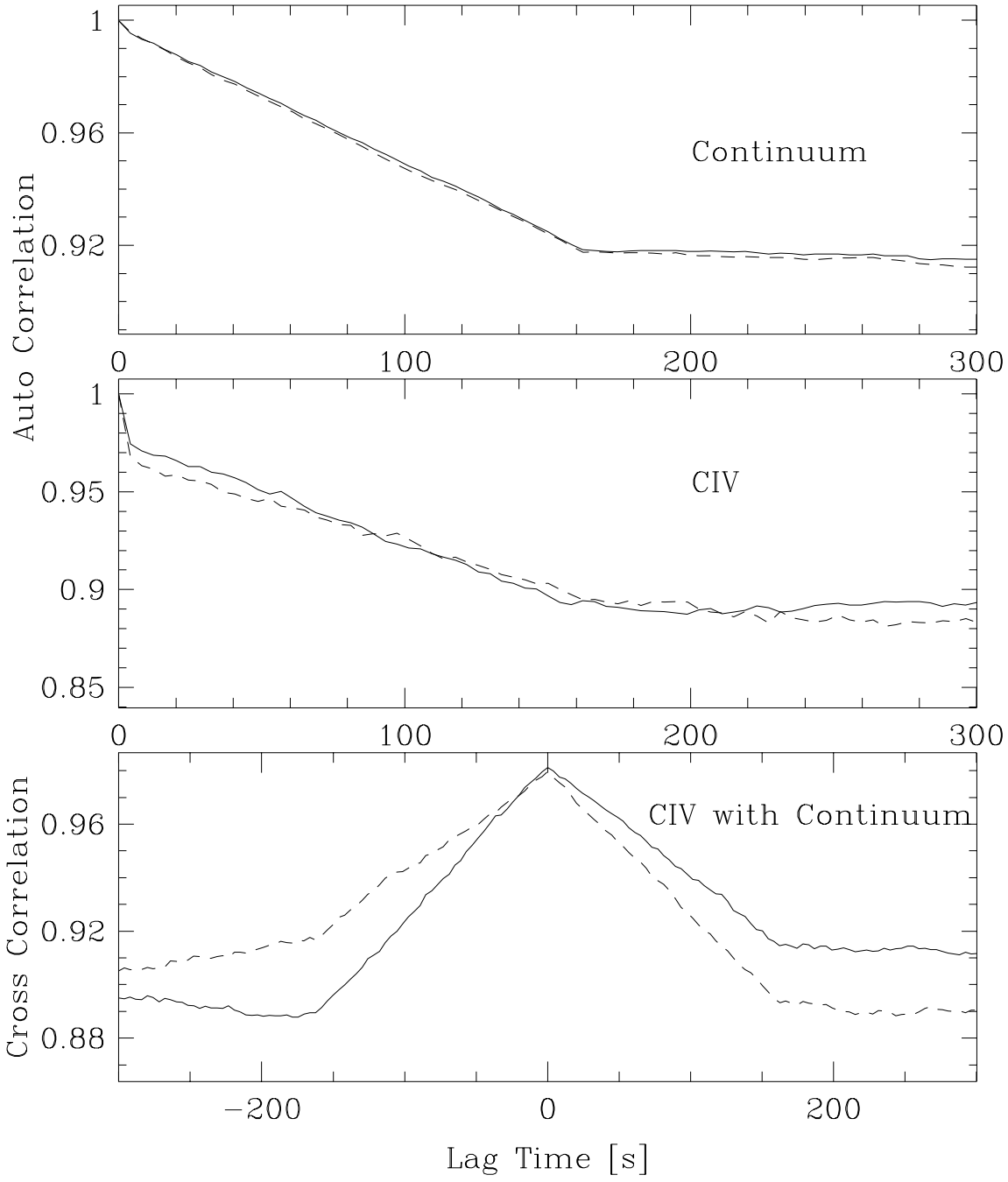

Fig. 5.— The autocorrelation of the continuum (top) and the C IV line (middle) and the cross correlation of the C IV with the continuum (bottom) for HST orbits 1 (solid) and 3 (dashed). The behavior of the other lines is similar to C IV line, although the other lines have inferior signal-to-noise. The autocorrelation shows evidence of a $\sim$ 2 min timescale. The line emission is highly correlated with the continuum, while there is no evidence of a time delay.

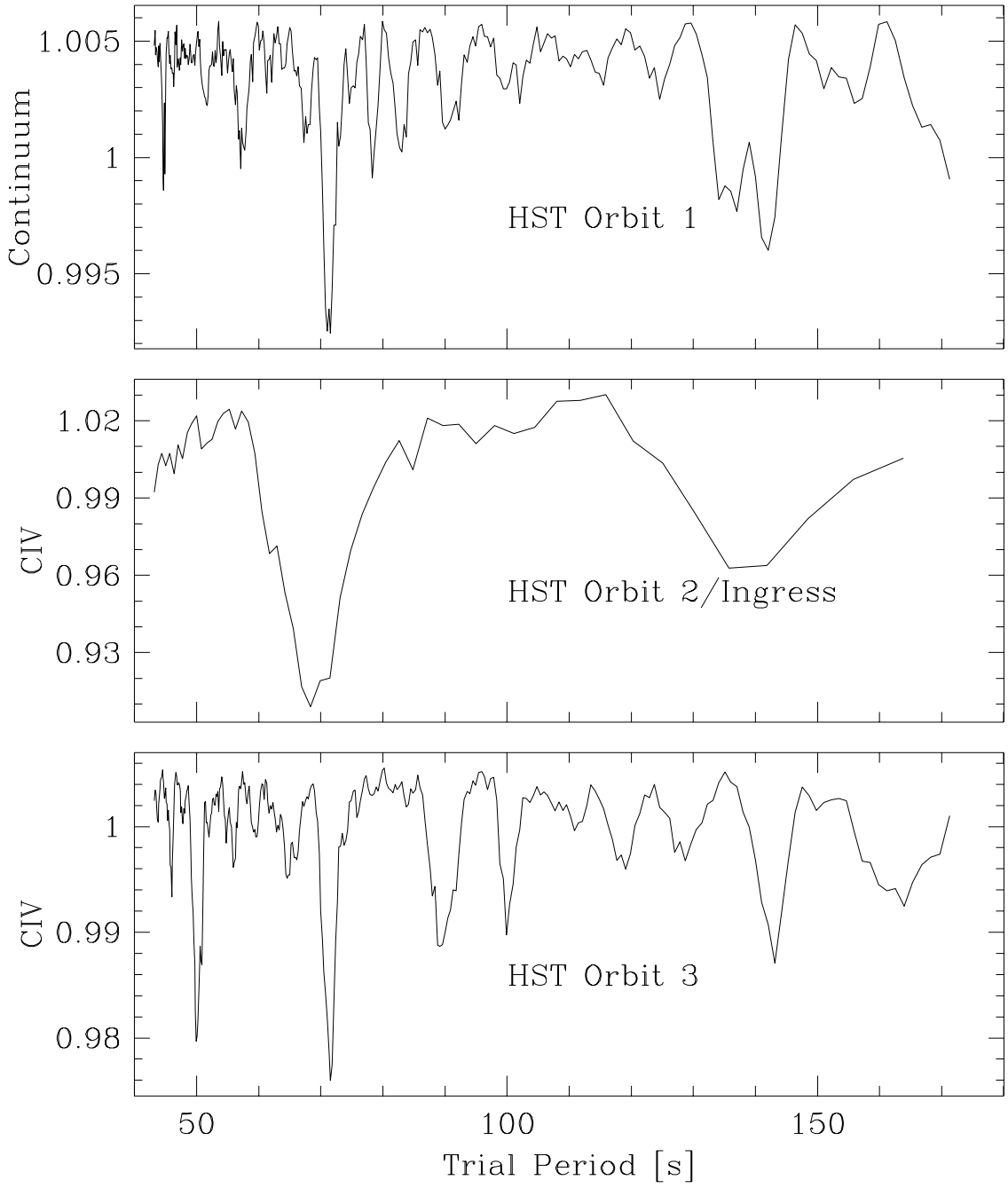

Fig. 6.— Pulsations at the 71 s period are clearly detected in two subsets: the UV continuum during the first HST orbit (top), and C IV during the third (bottom). During the eclipse ingress (middle) there is a weak, broad signal near the expected period.

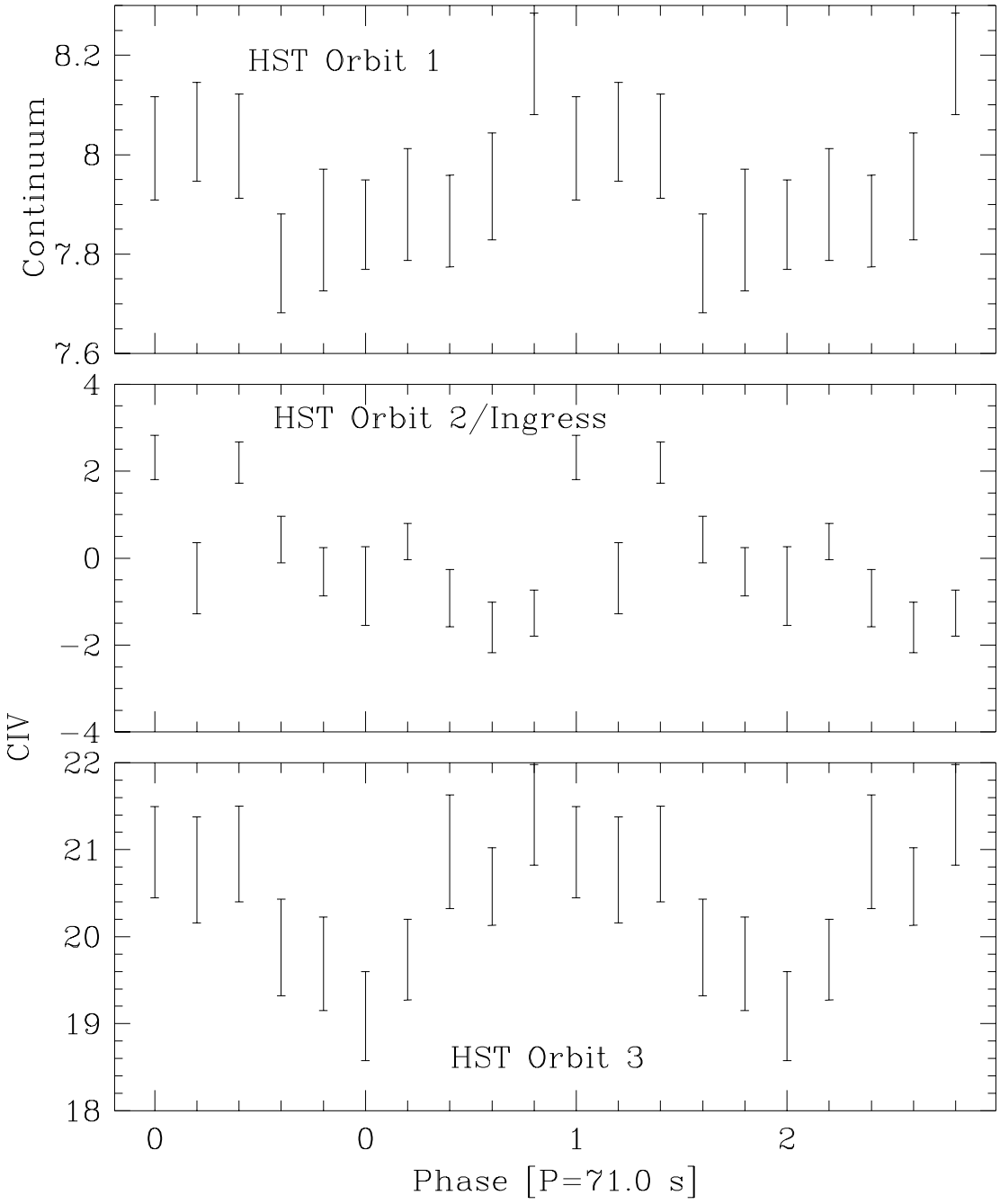

Fig. 7.— The continuum during the first HST orbit (top) in 10^{-15} ergs s^{-1} cm^{-2} Å^{-1}; C IV flux during the eclipse ingress after subtracting a linear fit (middle); and the C IV during the third HST orbit (bottom) in 10^{-13} ergs s^{-1} cm^{-2} all folded at a period of 71.0 s. The continuum and C IV during the third HST orbit both show clear variation that peaks at the same phase as the optical. The eclipse ingress pulsation data are less clear and likely not significant.